# Electro-deposited nano-webbed structures based on polyaniline/multi walled carbon nanotubes for enzymatic detection of organophosphates

Contents lists available at ScienceDirect

Food Chemistry

journal homepage: http://ees.elsevier.com

# Electro-deposited nano-webbed structures based on polyaniline/multi walled carbon nanotubes for enzymatic detection of organophosphates

Shalini Nagabooshanam [a], Alishba T. John [a], Shikha Wadhwa [a], Ashish Mathur [a,*], Satheesh Krishnamurthy [b], Lalit M. Bharadwaj [b]

[a] Amity Institute of Nanotechnology, Amity University, Sector-125, Noida 201301, UP, United Kingdom
[b] Nanoscale Energy and Surface Engineering, School of Engineering and Innovation, The Open University, Milton Keynes, MK 76AA, United Kingdom

ARTICLE INFO

*Keywords*
Organophosphates
Pesticides
Nano-composites
Polyaniline
Multi walled carbon nanotubes
Biosensor

ABSTRACT

We report the development of an ultrasensitive electrochemical sensor using polyaniline (PANi) and carboxyl functionalized multi-walled carbon nanotubes (fMWCNT) for the detection of organophosphates (OPs) in real samples. The sensor was tested in the linear concentration range of 10 ng/L to 120 ng/L. The limit of detection (LoD) was found to be 8.8 ng/L with sensitivity 0.41 mA/ng/L/cm$^2$ for chlorpyrifos (CPF); and 10.2 ng/L with sensitivity 0.58 mA/ng/L/cm$^2$ for methyl parathion (MP). The vegetable samples (cucumber) were also tested. The average % recovery for CPF and MP were found to be 98.05% and 96.63% respectively. The developed sensor showed stability for a period of 30 days. The interference of the sensor was studied with heavy metals (cadmium (Cd), chromium (Cr), lead (Pb), arsenic (As)) which was found to be < 10%. The developed sensor will play a major role in real-time monitoring of food products, leading to food safety.

## 1. Introduction

The use of OPs has resulted in multi-fold increase in crop production (Hassani et al., 2017). Although the use of OPs intended to control pest, consequently increasing yield; rampant usage of such chemicals has endangered life by interacting with non-target ecosystem such as water, soil, food, air, etc (Battaglin et al., 2016). Among other class of pesticides, organophosphates are of major concern, because they exhibit irreversible inhibition reaction with Acetylcholinesterase (AChE) enzyme (Arduini, Guidone, Amine, Palleschi, & Moscone, 2013). AChE is an active enzyme which aids in the conversion of neurotransmission agent acetylcholine into thiocholine and acetate (Darvesh et al., 2008). OPs enter human body through air, food or water sources causing an irreversible inhibition mechanism with AChE enzyme resulting in the accumulation of acetylthiocholine. This may cause severe health issues such as muscular dystrophy, neurological disorders, reproductive disorders, may lead to fatality (Costa, 2006). Therefore, detection and quantification of OPs with utmost precision is critically important. CPF and MP are most commonly used OPs in agriculture; even trace amounts are highly toxic and have high retention time within the food chain (Verma & Bhardwaj, 2015).

Conventional techniques such as Mass Spectroscopy (MS), Gas Chromatography-Mass Spectroscopy (GC–MS), High-Performance Liquid Chromatography (HPLC), Enzyme Linked Immuno-sorbent Assay (ELISA), other immunoassays are utilized for OPs detection (Di Ottavio et al., 2017; Grimalt & Dehouck, 2016). Aforementioned techniques require large sample volumes, sophisticated analytical laboratory, high operational cost and are time-consuming. Various analytical techniques for OP detection have been developed based on sophisticated electrochemical system using nanoparticles and composites to address the limitations of conventionally available detection techniques (Deng, Liu, Liu, Dong, & Li, 2016; Peng, Dong, Wei, Yuan, & Huang, 2017; Wei, Zeng, & Lu, 2014).

Recently, carbon nanotubes and conducting polymers have been used in sensing applications owing to their excellent properties including high surface area, electrical conductivity, chemical stability and electrochemical property (Alhans et al., 2018; Le, Kim, & Yoon, 2017; Moraes, Mascaro, Machado, & Brett, 2009). Considering all the above-mentioned properties, polyaniline (PANi) and MWCNTs based nanocomposite is a well-proven combination for electrochemical sensor fabrication. PANi and MWCNTs based nanocomposite provide excellent redox activity and stability (Cesarino, Moraes, & Machado, 2011). AChE immobilized on PANi and PANi-MWCNT composite have been reported for the detection of

* Corresponding author.
*E-mail address:* amathur@amity.edu (A. Mathur)

https://doi.org/10.1016/j.foodchem.2020.126784
Received 26 August 2019; Received in revised form 4 March 2020; Accepted 9 April 2020
Available online xxx
0308-8146/

various pesticides such as carbofuran, paraoxon, malathion, coumaphos, trichlorfon, aldicarb, methiocarb (Chen, Chen, & Du, 2010; Ivanov et al., 2002; Li, Zhao, Shi, Han, & Xiao, 2017). Previously reported techniques for PANi-fMWCNT composites require cumbersome synthesis procedures and use harmful chemicals.

In the present work, the main focus is to develop a simple, sensitive and low-cost sensing platform to detect OPs. We report the development of an ultrasensitive electrochemical sensor based on AChE enzyme immobilized PANi-fMWCNT hybrid nano webs. The hybrid PANi-fMWCNT is electrochemically synthesized by cyclic voltammetry (CV) technique, which provided in-line transfer of PANi-fMWNTs onto the conductive Indium Tin Oxide (ITO) surface without any intermediate agents. Electro polymerization technique allows rapid synthesis and in-situ electrochemical characterization with precise control to the deposited layer thickness, without any requirement of initiators or catalysts (del Valle et al., 2013). A simple two-step fabrication strategy was adopted, *i.e.* electro-polymerization of aniline monomers and carboxylated-MWCNT onto ITO surface resulting in hybrid nano webs followed by AChE enzyme immobilization which was covalently bound to the PANi - fMWCNT/ITO surface for a selective detection of OPs. The developed sensor was also tested with vegetable sample (cucumber) spiked with known amount of OPs.

## 2. Experimental section

### 2.1. Materials and chemicals

Acetylcholinesterase from electrophorus electricus (electric eel), acetyl thiocholine chloride (ATCl), chlorpyrifos (CPF), methyl parathion (MP), aniline, and oxalic acid were purchased from Sigma Aldrich. MWCNTs were purchased from Carbolex Inc. Ltd. US. Sodium chloride (NaCl), monobasic ($NaH_2PO_4{\cdot}2H_2O$), dibasic ($Na_2HPO_4$), potassium ferri hexa cyanide $K_3[Fe(CN)_6]$, potassium ferro hexa cyanide $K_4[Fe(CN)_6]$, sulphuric acid ($H_2SO_4$), nitric acid ($HNO_3$), and acetone were purchased from Fisher Scientific. Ethanol was purchased from Merck. All experiments were performed using Milli-Q Deionized (D.I) water having resistance 18.2 MΩ and analytical grade chemicals. ITO coated glass was purchased from TECHINSTRO, India (working area- 1 cm × 1 cm, resistivity of ~10 Ω/cm).

### 2.2. Apparatus and measurements

The surface of as-fabricated electrode was captured by Field Effect-Scanning Electron Microscopy (FE-SEM) Tescan MIRA II Oxford INCA PantaFETx3. Fourier Transform Infra-Red (FTIR) spectra were obtained by Frontier Perkin Elmer. Raman spectra were measured by micro Raman (Lab RAM system) equipped with $Ar^+$ 514.5 nm laser. Electrochemical analysis was performed by potentiostat/galvanostat (Multiautolab (MA204), Autolab) using three-electrode setup: platinum-counter electrode, Ag/AgCl (3 M KCl)-reference electrode and as-fabricated AChE/PANi-fMWCNT/ITO-working electrode. Phosphate Buffer Saline (PBS) (0.1 M), pH 7, containing 5 mM redox probe (Ferri-Ferro couple, $K[Fe(CN)_6]^{3-/4-}$) was used as electrolyte. Experiments were repeated three times to determine experimental error. LoD was calculated using 3σ rule [(3.3 × Standard Deviation /slope of the calibration plot] (Nagabooshanam et al., 2019).

### 2.3. Functionalization of MWCNT

In order to get better dispersion, as purchased MWCNTs were functionalized with carboxylic groups by acid reflux method. MWCNTs (0.3 g) were mixed in a solution containing 3:1 v/v ratio of $H_2SO_4$ and $HNO_3$ and refluxed at 80 °C for 12 h. Further, the centrifuged pellet was washed with D.I water and dried at 100 °C for 6 h in vacuum oven (Bachhav & Patil, 2015).

### 2.4. Fabrication of AChE/PANi-fMWCNT/ITO and electrocatalytic sensing performance

The stepwise fabrication of the working electrode is presented in Fig. 1. An aqueous solution containing 0.3 M oxalic acid, aniline (0.1 M) and fMWCNT (8 wt%) (Bachhav & Patil, 2015) were prepared as a pre-complex solution. PANi-fMWCT hybrid was electro-polymerized onto ITO for 10 cycles in the potential window of −0.8 V to 1.4 V at the scan rate of 50 mV/s. Pristine aniline was also electro-polymerized by the same procedure for comparison. Further, AChE enzyme (10 μL) was immobilized onto the PANi-fMWCNT/ITO electrode and the electrode was washed with PBS (pH 7) in order to remove any unbounded enzyme. Finally, the developed AChE/PANi-fMWCNT/ITO electrode was stored at 4 °C for further use.

The sensing mechanism of enzyme inhibition by pesticide (Fig. 1) can be explained as: AChE enzyme readily hydrolyzes acetylthiocholine resulting in generation of thiocholine and acetic acid. Thiocholine being electroactive produces a quantifiable change in current signal. Pesticides act as an inhibitor of AChE and hampers the above enzymatic reaction. The advantage of using a redox probe is to limit the overall applied potential and as a consequence, minimize electrochemical interference (Arduini, Amine, Moscone, & Palleschi, 2010). Inhibition of enzyme is calculated from Eq. (1); where $I_p$(before) and $I_p$(after) represents peak current before and after pesticide

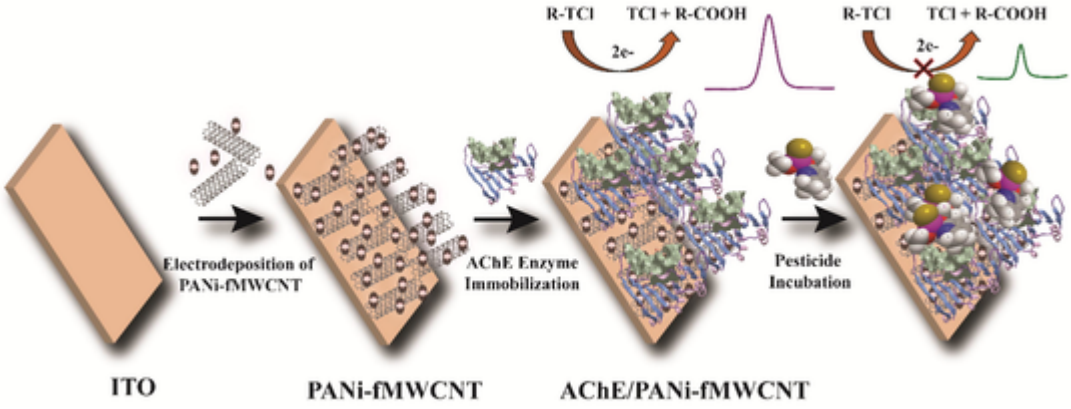


**Fig. 1.** Graphical representation of stepwise fabrication of working electrode (AChE/PANi-fMWCNT/ITO) and the reaction mechanism of enzyme inhibition by pesticides (R- Acetyl, TCl-Thiocholine).

incubation.

$$\%\text{Inhibition} = \frac{\text{Ip(before)} - \text{Ip(after)}}{\text{Ip(before)}} \times 100 \quad (1)$$

## 3. Results and discussion

### 3.1. Electrodeposition of PANi-fMWCNT nanocomposite on ITO

Cyclic voltammogram (Fig. S1) shows electrodeposition of PANi-fMWCNT hybrid structures onto ITO surface. There is an increase in current with successive CV cycles confirming electrodeposition. The electropolymerization process occurred under three noticeable voltages, *i.e.*, from generation of free radical cations at 0.3 V (a), facilitating oxidation at 0.5 V and 0.9 V (b and c) which correspond to head-to-tail dimer formation and thereafter, a direct transition from emeraldine phase to pernigraniline phase. The latter is reported to be more stable phase. (Pattananuwat & Aht-Ong, 2011).

### 3.2. FE-SEM analysis

The surface of PANi and PANi-fMWCNT hybrid electropolymerized onto ITO was probed by FE-SEM. Fig. 2A shows fMWCNT having length and diameter of 10–30 μm and 60–80 nm respectively. FE-SEM micrograph in Fig. 2B indicates the uniform deposition of pristine PANi granules in the size range 50 nm to 100 nm. In Fig. 2C, due to the addition of fMWCNT into the polymerization mixture, a hybrid nano-webbed structure with 50 nm to 100 nm PANi granules resulted in uniformly distributed network owing to π-π bonding at the backbone of carboxylated MWCNT and PANi. The coating of PANI on the outer surface of the CNT and the formation of the nano-webbed PANi-fMWCNT structures are evident from SEM image (Fig. 2C). Such an ordered hybrid of PANi-fMWCNT facilitates good electrical conductivity (Bachhav & Patil, 2015).

### 3.3. Raman and FTIR analysis

Fig. 3A shows Raman spectra of (i) fMWCNT, (ii) PANi, and (iii) PANi - fMWCNT nanocomposite. The D band at 1349 $cm^{-1}$ and sharp G band at 1579 $cm^{-1}$ corresponding to amorphous disoriented carbon structure and C—C bond stretching of fMWCNT (Filho et al., 2003; Mathur et al., 2012) can be observed. For PANi, characteristic peaks at 1195 $cm^{-1}$ and 1450 $cm^{-1}$ correspond to C—H bending and C═N stretching in benzenoid and quinoid structures (Lefrant, Baibarac, & Baltog, 2009). The band at 1373 $cm^{-1}$ and 1601 $cm^{-1}$ arise due to C—$N^{*+}$ stretching and C—C stretch of benzenoid ring which were found to be shifted to higher wavenumbers 1394 $cm^{-1}$ and 1616 $cm^{-1}$ for the hybrid material. This shift may be due to interaction of C— $N^{*+}$ group of PANi and –COO functional group on the fMWCNT (Yan, Han, Yang, & Tay, 2007). The amplification of Raman bands for PANi-fMWCNTs at 1616 $cm^{-1}$ and 1394 $cm^{-1}$ may be attributed to stress induced defects between the PANi and fMWCNT (Salvatierra, Oliveira, & Zarbin, 2010).

FTIR spectra of (i) PANi, (ii) PANi-fMWCNT, (iii) AChE immobilized PANi-fMWCNT are shown in Fig. 3B. For PANi, the N—H stretching vibrations, quinoid (Q) (C═C) and benzenoid (B) ring (C═C) appear at 3405 $cm^{-1}$, 1440 $cm^{-1}$ and 1580 $cm^{-1}$ respectively. The band at 1108 $cm^{-1}$ indicate aromatic C—H in-plane bending vibration respectively (Yan Li, Peng, Li, & Chen, 2012). The band at 1243 $cm^{-1}$ is assigned to C—$N^{+}$ stretching of radical cations. The peak at 730 $cm^{-1}$ is attributed to out-of-plane C—H bending vibration confirming the presence of polymer formation (Kulkarni & Kale, 2013). For PANi-fMWCNT, no prominent peak is observed, but a decrease in the peak intensity upon addition of fMWCNT

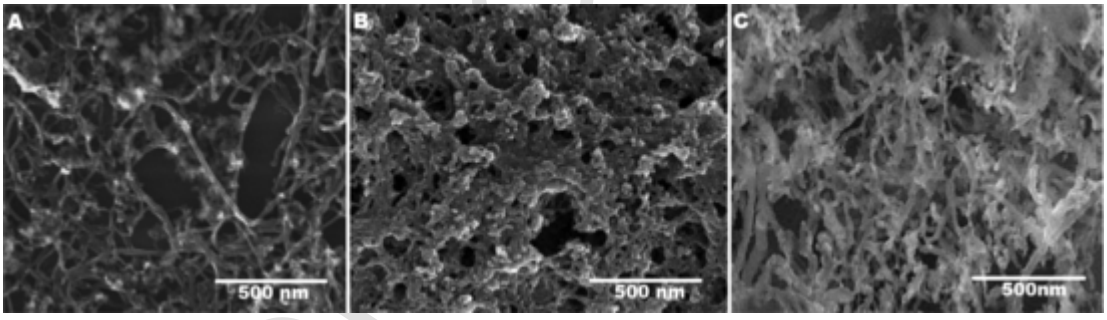


**Fig. 2.** Micrographic images probed using FE-SEM for A) fMWCNT, B) PANi/ITO and C) PANi-fMWCNT/ITO (scale bar showing 500 nm).

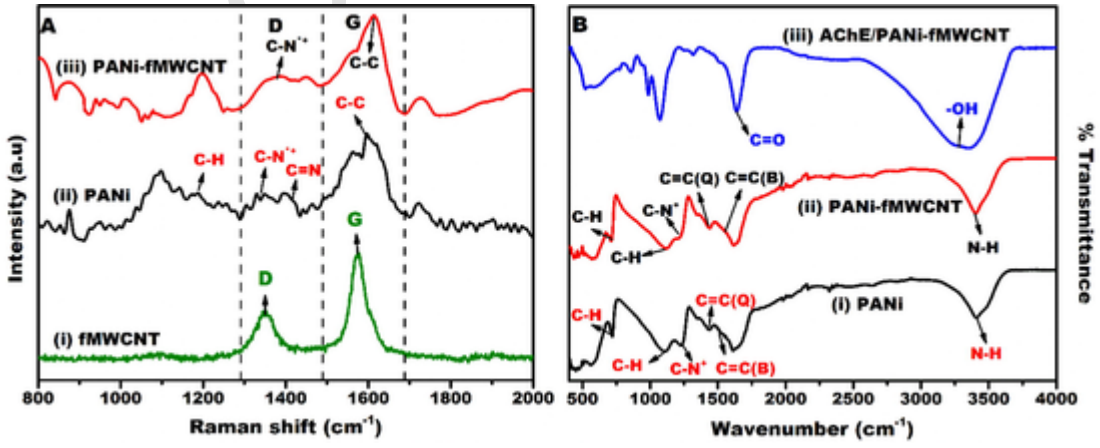


**Fig. 3.** A) Raman Spectra of the (i) fMWCNT, (ii) PANi and (iii) PANi-fMWCNT. B) FTIR Spectra of (i) PANi, (ii) PANi-fMWCNT and (iii) AChE/PANi-fMWCNT.

shows interaction between PANi and fMWCNT (Yadav, Kumar, & Pundir, 2011). The spectral bands at 1643 $cm^{-1}$ and 3297 $cm^{-1}$ are attributed to vibrations due to carbonyl and amide stretching (Du et al., 2007). These peaks signify the effective immobilization of AChE onto PANi-fMWCNT/ITO surface. FTIR spectra is also in agreement with the Raman analysis confirming the formation of PANi-fMWCNT hybrid structure and the functional groups required for effective enzyme immobilization which may lead to better sensing performance.

### 3.4. Electrochemical characterization of AChE/PANi-fMWCNT/ITO

The developed sensor was electrochemically characterized using CV and EIS at each step of sensor fabrication. In Fig. 4A, PANi-fMWCNT (i) modified ITO surface showed excellent enhancement in peak current ($I_{pa}$: 0.2 mA and $I_{pc}$: −0.2 mA) as compared to ITO electrode (ii) which showed moderate oxidation and reduction peaks ($I_{pa}$: 0.1 mA and $I_{pc}$: −0.1 mA). Owing to the conductive nature of PANi-fMWCNT, there is a significant enhancement of peak current due to the augmented charge transfer rate in the presence of redox probe (Cesarino et al., 2011). Furthermore, in case of AChE/PANi-fMWCNT/ITO electrode (iii), a clear decrease in redox peak current value ($I_{pa}$: 0.025 mA and $I_{pc}$: −0.025 mA) was observed, due to non-conducting nature of AChE enzyme, indicating the effective immobilization of AChE onto PANi-fMWCNT/ITO surface (Cui et al., 2018). From the EIS analysis (Fig. 4B), charge transfer resistance ($R_{ct}$) changes at each step of sensor development. $R_{ct}$ value for ITO electrode (28.49 kΩ) is 1.5 times higher in comparison to that of PANi-fMWCNT modified ITO electrode ($R_{ct}$ = 18.71 kΩ). This suggests faster electron transfer process leading to better electrochemical performance. After enzyme immobilization, the $R_{ct}$ value further increases to 33.59 kΩ which is almost 1.8 times higher than PANi-fMWCNT. This change in $R_{ct}$ value may correspond to the enzyme biomolecule layer which impedes interfacial charge transfer process (Cui et al., 2018; Song et al., 2017). Hence, electrochemical analysis shows a clear indication of successive modifications thereby confirming successful fabrication of the biosensor.

### 3.5. Effect of applied scan rate

From cyclic voltammogram of AChE/PANi-fMWCNT/ITO electrode (Fig. S2A), the regression line equation for anodic peak is expressed as y = 0.012 × + 0.008, whereas for cathodic peak as y = −0.013 × −0.01, with regression coefficient of 0.99. The anodic and cathodic peak current linearly increases with increase in applied scan rate as observed in Fig. S2B. This suggests that the redox process is diffusion mediated, as desired for better sensing performance.

### 3.6. Electro-catalytic and analytical sensing performance

Analytical sensing was carried out using a probe solution containing 100 μM ATCl within the potential window of −0.8 V to +1.2 V at the scan rate of 100 mV/s. The notable rise of peak current in the presence of ATCl is attributed to the electro-catalytic reaction between the enzyme and ATCl (Fig. S3). The hydroxyl groups present within the enzyme reacts with ATCl, converting it into thiocholine and in the process generate electrons responsible for electro activity (Mogha, Sahu, Sharma, Sharma, & Masram, 2016). From Fig. 5A and 5C, it is observed that with increase in concentration of CPF and MP, the current decreases. The active cationic sites present in AChE enzyme binds to the phosphate groups present in CPF and MP, causing an irreversible binding reaction (Uniyal & Sharma, 2018). For both CPF and MP sensing, the peak current decreases and % of inhibition increases linearly, with increase in the pesticide concentration. The linearly fitted regression equations derived for both CPF and MP are shown in Fig. 5B and 5D. The intercept and slope values for CPF obtained are 41.88 ± 2.8 and 0.41 ± 0.03 respectively, with regression fitted line equation $y = 41.88 + 0.41 \times C_{CPF}$ and $r^2$ value of 0.97. For MP the intercept and slope values were 21.05 ± 5.66 and 0.58 ± 0.06 respectively with regression fitted line equation $y = 21.05 + 0.58 \times C_{MP}$ and $r^2$ value of 0.94. As per 3σ rule, LoD was calculated to be 8.8 ng/L for CPF and 10.2 ng/L for MP. The sensitivity of the developed sensor for CPF and MP were 0.41 mA/ng/ $L/cm^2$ and 0.58 mA/ng/L $/cm^2$ respectively. The LoD achieved by the developed sensor is lower than that of permissible Maximum Residue Levels (MRL) values of 0.05 ppm and 0.20 ppm for CPF and MP as per European pesticides database (EU Pesticides database - European Commission, n.d.). The response time of the developed sensor is found to be 45 s. The AChE/PANi-fMWCNT sensor is compared with other reported AChE based sensors (Table S1), the better LoD and sensitivity is achieved due to the synergistic effect of PANi-fMWCNT hybrid complimented with enhanced electrochemical properties, good electron transfer rate and enhanced surface properties for enzyme immobilization. Thus, the improved sensing performance of AChE/PANi-fMWCNT is attributed to PANi and fMWCNT amalgamation and readily available carboxyl functional groups. The porous nano-webbed architecture enhances the surface area attributing to faster electron transfer kinetics. The available car-

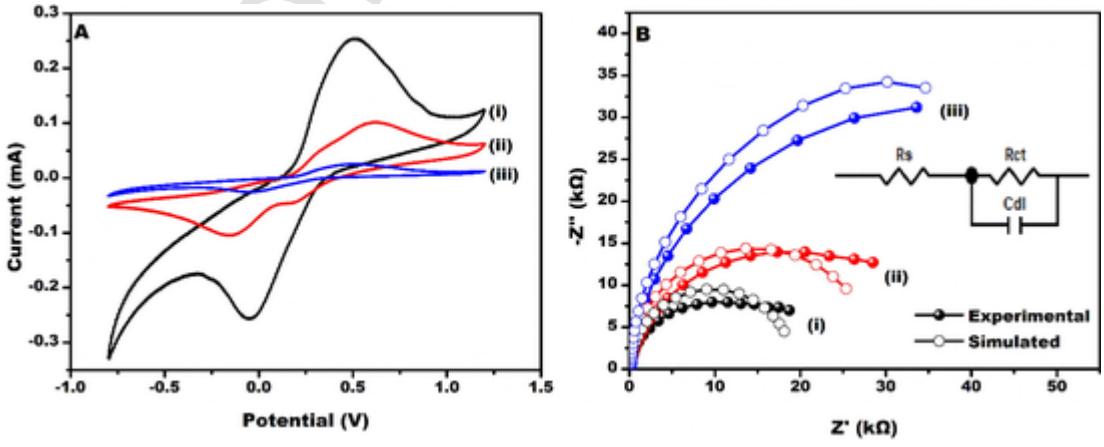


**Fig. 4.** Electrochemical characterization at each step of modification of electrode (i) PANi-fMWCNT, (ii) ITO, (iii) AChE/PANi-fMWCNT/ITO by A) CV scanning at a rate of 100 mV/s in the potential window of −0.8 V to + 1.2 V and B) Electrochemical Impedance Spectroscopy (EIS) in the frequency range 100 Hz to 100 KHz using 10 mV AC perturbation.

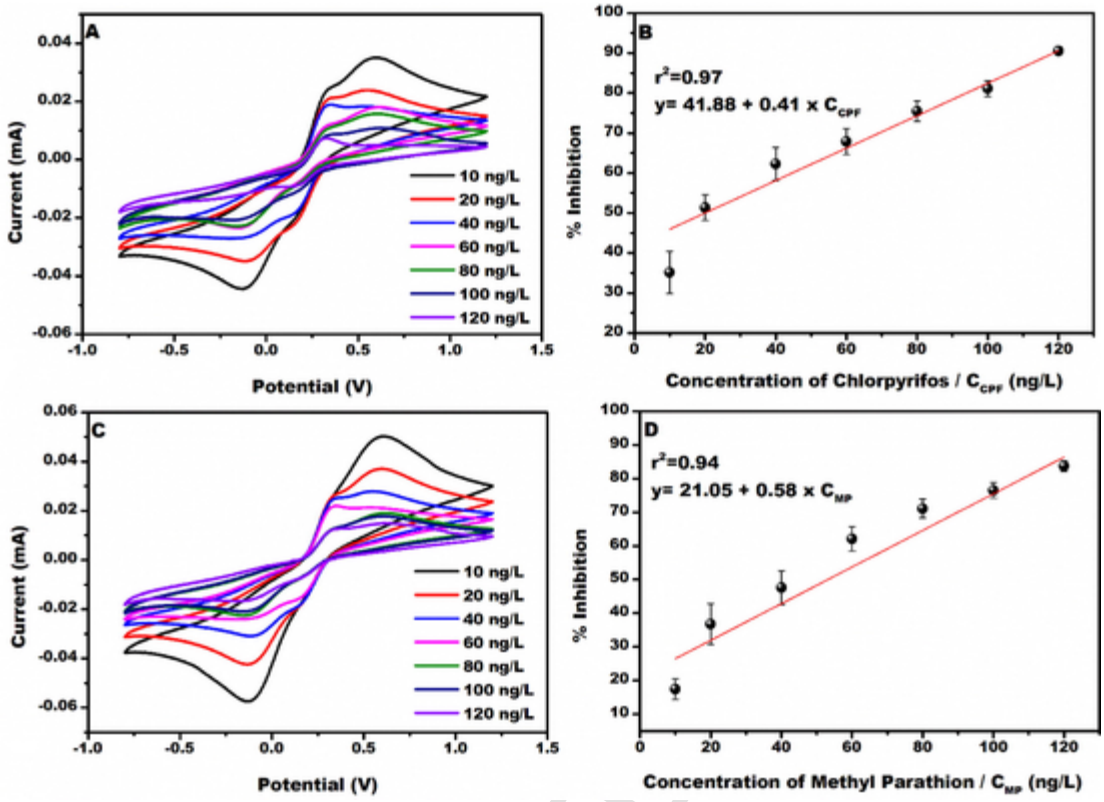


**Fig. 5.** CV response for different concentrations of A) CPF C) MP in the concentration range 10–120 ng/L. Calibration plot for different concentrations of B) CPF D) MP showing linear regression line equation.

boxyl functional groups facilitate AChE enzyme immobilization due to which, the sensor exhibits a lower detection limit, wider linear range and better sensitivity.

### *3.7. Interference and stability studies*

Heavy metals (Cr, Cd, As, Pb) make their way into the food chain through metal contaminated soil, wastewater irrigation, post-harvest treatments and polluted environments and can be readily absorbed by fruits and vegetables (Abdel-Rahman, Ahmed, & Marrez, 2018; Elbagermi, Edwards, & Alajtal, 2012). The presence of heavy metals in fruits and vegetables may interfere with the performance of the developed pesticide sensor and therefore, it is of utmost importance to confirm specificity of the developed sensor. As per the reports, the MRLs of heavy metals such as Cr and Pb are 0.5 mg/kg and 0.2 mg/kg in various fruit and vegetable sources (Elbagermi et al., 2012; Zhao, Li, Gao, & Li, 2017). In order to investigate their interference with pesticide detection, heavy metal solutions were prepared with pesticide mixtures. The developed sensor was tested for MP detection in the presence of heavy metals at concentration of 10 ng/L (Fig. S4A). Hence, no significant interference of heavy metal was detected.

The overall stability of the developed sensor was monitored at five-day interval over a month (Fig. S4B), after which the sensor's activity was found to be decreased. The average peak current ($I_p$) over a period of 30 days was found to be 0.038 ± 0.003(average peak current ± SD). About 17% decrease in the current response was observed after 30 days suggesting the sensor's stability/shelf-life for 30 days. The decrease in sensor's activity may be attributed to the enzyme degradation after prolonged storage, resulting in lower charge transfer kinetics.

The inhibition effect of another class of pesticides not containing phosphate groups (Cartap Hydrochloride (CHCl), a chlorinated class of pesticide) has also been tested by the presently developed sensor. CHCl (at 100 ng/L concentration) demonstrated merely 8.5% inhibition effect on the activity of AChE enzyme (Fig. S5). Therefore, other class of pesticides may show some inhibition effect on AChE enzyme activity, however, a detailed study on various class of pesticides must be undertaken to conclude the effect of inhibition on enzyme activity which is beyond the scope of this work.

### *3.8. Pesticide determination in vegetable sample*

The pertinence of the developed sensor in real samples was also verified. Cucumber juice was spiked with known concentrations (20 ng/L and 120 ng/L) of CFP and MP. Current response was measured by CV for CPF and MP spiked cucumber samples (Fig. S6). The standard calibration plots as shown in Fig. 5B and 5D were used to calculate the concentration of spiked pesticides in cucumber sample. The developed sensor shows a good recovery of spiked CPF and MP with RSD less than 9% (Table 1), which affirms the ability of the sensor for pesticide detection in real field samples. In order to

**Table 1**
Real sample analysis by spiking known amount of OPs in cucumber vegetable sample (RSD-Relative Standard Deviation).

| Sample OP | Added (ng/L) | Found (ng/L) | % Recovery | % RSD (n = 3) |
|---|---|---|---|---|
| CPF | 120 | 118.4 | 98.6 | 8.3 |
| CPF | 20 | 19.5 | 97.5 | 6.2 |
| MP | 120 | 119.7 | 99.75 | 7.9 |
| MP | 20 | 18.7 | 93.5 | 3.6 |

validate the present sensor performance, HPLC analysis was performed and good correlation of $r^2 = 0.996$ is found (Fig. S7 and Table S2).

## 4. Conclusion

A facile approach to fabricate nano-webbed structures of PANi-fMWCNTs onto ITO substrate is developed for the detection of OPs. Electrochemical polymerization for PANi-fMWCNT nanocomposite synthesis provides a rapid electrode development process along with better surface properties. The developed sensor was tested with two analytes (CPF and MP) in the linear concentration range of 10 ng/L to 120 ng/L. The LoD was found to be 8.8 ng/L and 10.2 ng/L for CPF and MP with sensitivity of 0.41 mA/ng/L/cm$^2$ and 0.58 mA/ng/L/cm$^2$ respectively. The sensor was also tested with heavy metals for interference which was found to be <10%. The spiked vegetable samples were also tested by the sensor with good accuracy. The developed sensor has a shelf-life of 30 days. The sensor can further be utilized for on-field detection for OPs detection in fruit and vegetable samples.

## Authors contribution

SN and AJ performed the electrochemical sensing experiments and data analysis. SN and AM provided the fabrication and characterization of biosensing platform. SW, AM and SK supervised the overall experiments and data analysis; LMB, AM and SK provided valuable insights for compilation of the overall manuscript. All authors contributed equally to the manuscript.

## Declaration of Competing Interest

The authors declare that they have no known competing financial interests or personal relationships that could have appeared to influence the work reported in this paper.

## Acknowledgments

Authors are grateful for the financial support from ICAR through NASF funded project NASF/Nano-5020/2016-17. Authors would also like to acknowledge support from NIBEC, Ulster University U.K. for material characterization. Authors would also like to acknowledge support from IARI, New Delhi for real sample analysis.

## Appendix A. Supplementary data

Supplementary data to this article can be found online at https://doi.org/10.1016/j.foodchem.2020.126784.

## References

Abdel-Rahman, G N, Ahmed, M B M, & Marrez, D A (2018). Reduction of heavy metals content in contaminated vegetables due to the post-harvest treatments. Egyptian Journal of Chemistry, 61, 1031–1037. doi:10.21608/ejchem.2018.3624.1303.

Alhans, R, Singh, A, Singhal, C, Narang, J, Wadhwa, S, & Mathur, A (2018). Comparative analysis of single-walled and multi-walled carbon nanotubes for electrochemical sensing of glucose on gold printed circuit boards. Materials Science and Engineering: C, 90, 273–279. doi:10.1016/J.MSEC.2018.04.072.

Arduini, F, Amine, A, Moscone, D, & Palleschi, G (2010). Biosensors based on cholinesterase inhibition for insecticides, nerve agents and aflatoxin B1 detection (review). Microchimica Acta, 170, 193–214. doi:10.1007/s00604-010-0317-1.

Arduini, F, Guidone, S, Amine, A, Palleschi, G, & Moscone, D (2013). Acetylcholinesterase biosensor based on self-assembled monolayer-modified gold-screen printed electrodes for organophosphorus insecticide detection. Sensors and Actuators, B: Chemical, 179, 201–208. doi:10.1016/j.snb.2012.10.016.

Bachhav, S G, & Patil, D R (2015). Synthesis and characterization of polyaniline-multiwalled carbon nanotube nanocomposites and its electrical percolation behavior. American Journal of Materials Science, 5, 90–95. doi:10.5923/j.materials.20150504.03.

Battaglin, W A, Smalling, K L, Anderson, C, Calhoun, D, Chestnut, T, & Muths, E (2016). Potential interactions among disease, pesticides, water quality and adjacent land cover in amphibian habitats in the United States. Science of The Total Environment, 566–567, 320–332. doi:10.1016/J.SCITOTENV.2016.05.062.

Cesarino, I, Moraes, F C, & Machado, S A S (2011). A biosensor based on polyaniline-carbon nanotube core-shell for electrochemical detection of pesticides. Electroanalysis, 23, 2586–2593. doi:10.1002/elan.201100161.

Chen, D, Chen, C, & Du, D (2010). Detection of organophosphate pesticide using polyaniline and carbon nanotubes composite based on acetylcholinesterase inhibition. Journal of Nanoscience and Nanotechnology, 10, 5662–5666. doi:10.1166/jnn.2010.2477.

Costa, L G (2006). Current issues in organophosphate toxicology. Clinica Chimica Acta, 366, 1–13. doi:10.1016/j.cca.2005.10.008.

Cui, H F, Wu, W W, Li, M M, Song, X, Lv, Y, & Zhang, T T (2018). A highly stable acetylcholinesterase biosensor based on chitosan-TiO2-graphene nanocomposites for detection of organophosphate pesticides. Biosensors and Bioelectronics, 99, 223–229. doi:10.1016/j.bios.2017.07.068.

Darvesh, S, Darvesh, K V, McDonald, R S, Mataija, D, Walsh, R, & Mothana, S, et al. (2008). Carbamates with differential mechanism of inhibition toward acetylcholinesterase and butyrylcholinesterase. Journal of Medicinal Chemistry, 51, 4200–4212. doi:10.1021/jm8002075.

del Valle, M A, Canales, L I, Ramos, A, Díaz, F R, Hernández, L A, & Armijo, F, et al. (2013). Electropolymerization and morphologic characterization of α-tetrathiophene. International Journal of Electrochemical Science, 8, 1422–1433.

Deng, Y, Liu, K, Liu, Y, Dong, H, & Li, S (2016). An novel acetylcholinesterase biosensor based on nano-porous pseudo carbon paste electrode modified with gold nanoparticles for detection of methyl parathion. Journal of Nanoscience and Nanotechnology, 16, 9460–9467. doi:10.1166/jnn.2016.13059.

Di Ottavio, F, Della Pelle, F, Montesano, C, Scarpone, R, Escarpa, A, & Compagnone, D, et al. (2017). Determination of pesticides in wheat flour using microextraction on packed sorbent coupled to ultra-high performance liquid chromatography and tandem mass spectrometry. Food Analytical Methods, 10, 1699–1708. doi:10.1007/s12161-016-0720-2.

Du, D, Huang, X, Cai, J, Zhang, A, Ding, J, & Chen, S (2007). An amperometric acetylthiocholine sensor based on immobilization of acetylcholinesterase on a multiwall carbon nanotube-cross-linked chitosan composite. Analytical and Bioanalytical Chemistry, 387, 1059–1065. doi:10.1007/s00216-006-0972-6.

Elbagermi, M A, Edwards, H G M, & Alajtal, A I (2012). Monitoring of heavy metal content in fruits and vegetables collected from production and market sites in the Misurata area of Libya. ISRN Analytical Chemistry, 2012, 1–5. doi:10.5402/2012/827645.

EU Pesticides database - European Commission. (n.d.). Retrieved January 13, 2020, from https://ec.europa.eu/food/plant/pesticides/eu-pesticides-database/public/?event=homepage&language=EN.

Filho, A G S, Jorio, A, Samsonidze, G G, Dresselhaus, G, Saito, R, & Dresselhaus, M S (2003). Raman spectroscopy for probing chemically/physically induced phenomena in carbon nanotubes. Nanotechnology, 14, 1130–1139. doi:10.1088/0957-4484/14/10/311.

Grimalt, S, & Dehouck, P (2016). Review of analytical methods for the determination of pesticide residues in grapes. Journal of Chromatography A, 1433, 1–23. doi:10.1016/J.CHROMA.2015.12.076.

Hassani, S, Momtaz, S, Vakhshiteh, F, Maghsoudi, A S, Ganjali, M R, & Norouzi, P, et al. (2017). Biosensors and their applications in detection of organophosphorus pesticides in the environment. Archives of Toxicology, 91, 109–130. doi:10.1007/s00204-016-1875-8.

Ivanov, A N, Lukachova, L V, Evtugyn, G A, Karyakina, E E, Kiseleva, S G, & Budnikov, H C, et al. (2002). Polyaniline-modified cholinesterase sensor for pesticide determination. Bioelectrochemistry, 55, 75–77. doi:10.1016/S1567-5394(01)00163-3.

Kulkarni, M V, & Kale, B B (2013). Studies of conducting polyaniline (PANI) wrapped-multiwalled carbon nanotubes (MWCNTs) nanocomposite and its application for optical pH sensing. Sensors and Actuators B: Chemical, 187, 407–412. doi:10.1016/J.SNB.2012.12.106.

Le, T H, Kim, Y, & Yoon, H (2017). Electrical and electrochemical properties of conducting polymers. Polymers, 9, 150. doi:10.3390/polym9040150.

Lefrant, S, Baibarac, M, & Baltog, I (2009). Raman and FTIR spectroscopy as valuable tools for the characterization of polymer and carbon nanotube based composites. Journal of Materials Chemistry, 19, 5690. doi:10.1039/b821136a.

Li, Yan, Peng, H, Li, G, & Chen, K (2012). Synthesis and electrochemical performance of sandwich-like polyaniline/graphene composite nanosheets. European Polymer Journal, 48, 1406–1412. doi:10.1016/j.eurpolymj.2012.05.014.

Li, Yanping, Zhao, R, Shi, L, Han, G, & Xiao, Y (2017). Acetylcholinesterase biosensor based on electrochemically inducing 3D graphene oxide network/multi-walled carbon nanotube composites for detection of pesticides. RSC Advances, 7, 53570–53577. doi:10.1039/c7ra08226f.

Mathur, A, Roy, S S, Wadhwa, S, Ray, S C, Hazra, K, & Misra, D S, et al. (2012). Substrate effects on the growth of multiwalled carbon nanotubes by thermal chemical vapor deposition. Advanced Science Letters, 7, 21–26. doi:10.1166/asl.2012.3314.

Mogha, N K, Sahu, V, Sharma, M, Sharma, R K, & Masram, D T (2016). Biocompatible ZrO 2 - reduced graphene oxide immobilized AChE biosensor for chlorpyrifos detection. Materials and Design, 111, 312–320. doi:10.1016/j.matdes.2016.09.019.

Moraes, F C, Mascaro, L H, Machado, S A S, & Brett, C M A (2009). Direct electrochemical determination of carbaryl using a multi-walled carbon nanotube/cobalt phthalocyanine modified electrode. Talanta, 79, 1406–1411. doi:10.1016/j.talanta.2009.06.013.

Nagabooshanam, S, Roy, S, Mathur, A, Mukherjee, I, Krishnamurthy, S, & Bharadwaj, L M (2019). Electrochemical micro analytical device interfaced with

portable potentiostat for rapid detection of chlorpyrifos using acetylcholinesterase conjugated metal organic framework using Internet of things. Scientific Reports, 9, 1–9. doi:10.1038/s41598-019-56510-y.

Pattananuwat, P, & Aht-Ong, D (2011). Electrochemical Synthesis of sensitive layer of polyaniline/multi wall carbon nanotube composite. Materials Science Forum, 695, 336–339. doi:10.4028/www.scientific.net/msf.695.336.

Peng, L, Dong, S, Wei, W, Yuan, X, & Huang, T (2017). Synthesis of reticulated hollow spheres structure $NiCo_2S_4$ and its application in organophosphate pesticides biosensor. Biosensors and Bioelectronics, 92, 563–569. doi:10.1016/J.BIOS.2016.10.059.

Salvatierra, R V, Oliveira, M M, & Zarbin, A J G (2010). One-pot synthesis and processing of transparent, conducting, and freestanding carbon nanotubes/polyaniline composite films. Chemistry of Materials, 22, 5222–5234. doi:10.1021/cm1012153.

Song, D, Li, Y, Lu, X, Sun, M, Liu, H, & Yu, G, et al. (2017). Palladium-copper nanowires-based biosensor for the ultrasensitive detection of organophosphate pesticides. Analytica Chimica Acta, 982, 168–175. doi:10.1016/j.aca.2017.06.004.

Uniyal, S, & Sharma, R K (2018). Technological advancement in electrochemical biosensor based detection of Organophosphate pesticide chlorpyrifos in the environment: A review of status and prospects. Biosensors and Bioelectronics, 116, 37–50. doi:10.1016/j.bios.2018.05.039.

Verma, N, & Bhardwaj, A (2015). Biosensor technology for pesticides—A review. Applied Biochemistry and Biotechnology, 175, 3093–3119. doi:10.1007/s12010-015-1489-2.

Wei, M, Zeng, G, & Lu, Q (2014). Determination of organophosphate pesticides using an acetylcholinesterase-based biosensor based on a boron-doped diamond electrode modified with gold nanoparticles and carbon spheres. Microchimica Acta, 181, 121–127. doi:10.1007/s00604-013-1078-4.

Yadav, S, Kumar, A, & Pundir, C S (2011). Amperometric creatinine biosensor based on covalently coimmobilized enzymes onto carboxylated multiwalled carbon nanotubes/polyaniline composite film. Analytical Biochemistry, 419, 277–283. doi:10.1016/J.AB.2011.07.032.

Yan, X Bin, Han, Z J, Yang, Y, & Tay, B K (2007). Fabrication of carbon nanotube-polyaniline composites via electrostatic adsorption in aqueous colloids. Journal of Physical Chemistry C, 111, 4125–4131. doi:10.1021/jp0651844.

Zhao, X.-G., Li, B., Gao, M.-D., & Li, Y. (2017). Detection and Analysis of Heavy Metals in Vegetables in Xinzhu Vegetable Base, 94, 252–254. https://doi.org/10.2991/icsd-16.2017.55.